Optimization of the diffraction efficiency in non-uniform gratings in sillenite crystals ($Bi_{12}SiO_{20}$ and $Bi_{12}TiO_2$) considering the variation of fringe period, optical activity and polarization angles in a strong non-linear regime

G. González and A. Zúñiga

Escuela Superior de Física y Matemáticas, Instituto Politécnico Nacional, México,
Edificio 9, Unidad profesional Adolfo López Mateos,
México D.F., 07730, México.

F. Magaña

Instituto de Física, Universidad Nacional Autónoma de México,
Apartado Postal 20-364, México D.F. 0100, México,
e-mail: fernando@fisica.unam.mx

We included the non-uniformity of the grating and of the magnitude and phase of light modulation throughout the sample thickness to optimize the diffraction efficiency. The variation of fringe period, optical activity, birefringence, absorption of light, and polarization angle were considered. We studied strong nonlinear conditions and two crystal orientations one is with the grating vector parallel to the face [001] and the other is with the grating vector perpendicular to the same face. We included applied fields There is a complex relationship among all these parameters, and the prediction of the conditions for the optimum value of the diffraction efficiency is complicated. We report the optimal sample thickness for different situations, considering two wavelengths for reading: green (532 nm) and red (632 nm).

Keywords: Photorefractive gratings; refractive index; beam coupling; energy exchange; non-linear optics.

Incluimos la no uniformidad de la rejilla y de la magnitud y de la fase de la modulación de la luz a lo largo del espesor de la muestra, para optimizar la eficiencia de difracción, considerando la variación del período de la rejilla, condiciones fuertemente no lineales, actividad óptica, birrefringencia, absorción, ángulo de polarización, campos aplicados y dos orientaciones del cristal: el vector de la rejilla paralelo y perpendicular a la dirección [001]. Existe una relación compleja entre todos estos parámetros y la predicción de las condiciones óptimas para la eficiencia de difracción es complicada. Reportamos el espesor óptimo de la muestra en diferentes circunstancias, utilizando dos diferentes longitudes de onda para la lectura: verde (532 nm) y roja (632 nm).

Descriptores: Rejillas fotorrefractivas; índice de refracción; acoplamiento de haces; intercambio de energía; óptica no lineal.

PACS: 42.65.-k; 42.70.-a; 42.70.Nq.

1. Introduction

The cubic crystals of the sillenite family (BSO, BGO and BTO) have been studied extensively. They have high sensitivity, unlimited recyclability and long holographic storage times with a good potential for technological use [1-3]. They have a strong enough response only when an external electric field is applied during the photorefractive grating recording. These materials have a faster response than barium titanate or lithium niobate, and show a lower gain because of the low value of their electro-optic coefficient. Sillenite crystals are optically active and linearly birefringent in the presence of an electric field. They exhibit complex polarization effects [4].

When a large absorption coefficient is present in the photorefractive material, the light waves decay very rapidly inside the sample. In this case, the energy exchange as well as the spatial non-uniformity of the grating is irrelevant.

However, for thick sillenite samples with no very large absorption coefficients [5, 6] under a non-linear regime, there is a strong beam coupling. In this case there is a spatial redistribution of the light intensity pattern that changes the light modulation across the crystal In this way the grating is spatially non-uniform and its amplitude and phase change throughout the sample thickness In previous work it was shown that the spatial variation of the grating and of the light modulation has a great influence on the energy exchange between the beams [7, 8].

In this work we studied thick sillenite crystals, where the effects of beam coupling become significant. We considered non-moving transmission gratings under an applied field and strong non-linear conditions. For these systems we calculated the diffraction efficiency considering the non-uniformity of the gratings along sample thickness. We considered the variation of fringe period. We included optical activity, birefringence, and absorption of light. Several values of light modulation and polarization angles of the incident beams are considered. Two crystal orientations are considered: the first one is with the grating vector parallel to the face [001] and the second one is with the grating vector perpendicular to the same face.

We started by numerically solving the set of non-linear material rate differential equations [9,10] to find the full space charge field for each of the values of the grating period, Λ, we have considered: 1, 2, 3, 4, 5, 7 and 10 microns. In each case we took several values of the light modulation at the surface of the sample, m_0 between zero and one. Then we performed the Fourier decomposition of the calculated overall space charge fields for each of the considered cases to obtain the amplitude, E_1 of its fundamental Fourier component and its phase, Φ. This information was required to obtain the grating strength and its phase, which are necessary to solve the beam coupling equations, as functions of light modulation.

Then we followed a vector approach [11-14] to express the two wave coupling equations. The solutions to the corresponding two sets of beam coupling equations were obtained numerically considering the non-uniformity of light modulation and of the grating amplitude and its phase along the sample thickness. We used two wavelengths for reading: green (532 nm), and red (632 nm). The Bragg condition is always satisfied.

2.   Coupled wave equations

We considered the interaction of two, plane, monochromatic, linearly polarized electromagnetic waves $\vec{A}_1(\vec{r})$ and $\vec{A}_2(\vec{r})$ that propagate inside the sample. Each field has two components: one, along $\hat{u}_\zeta$ perpendicular to the plane of incidence $(x-z)$ and the other, along $\hat{u}_\xi$ parallel to the same plane. The total light field can then be written as the superposition of these two:

$$\vec{A}(\vec{r}) = \vec{A}_1(\vec{r})\exp(-i\vec{k}_1 \bullet \vec{r} + \Psi_1)$$
$$+ \vec{A}_2(\vec{r})\exp(-i\vec{k}_2 \bullet \vec{r} + \Psi_2) \qquad (1)$$

where $\vec{k}_1$ and $\vec{k}_2$ are the corresponding wave vectors, Ψ_1, Ψ_2 represent the phases of the two light waves, and

$$\vec{A}_1(\vec{r}) = \vec{A}_{1\xi}(\vec{r})\hat{u}_\xi + A_{1\varsigma}(\vec{r})\hat{u}_\varsigma;$$
$$\vec{A}_2(\vec{r}) = A_{2\xi}(\vec{r})\hat{u}_\xi + A_{2\varsigma}(\vec{r})\hat{u}_\varsigma$$

The light modulation $m(\vec{r})$ varies along the sample thickness according to:

$$m(\vec{r}) = \frac{2[A_{1\xi}(\vec{r})A_{2\xi}(\vec{r})^* + A_{1\varsigma}(\vec{r})^*A_{2\varsigma}(\vec{r})]}{I_0} \qquad (2)$$

where

$$I_0 = \left|\vec{A}_1(0)\right|^2 + \left|\vec{A}_2(0)\right|^2$$

With the interference pattern in the photorefractive material the light excites electrons to the conduction band, which migrate due to diffusion, and drift from the bright to the dark parts of the crystal, where they are captured by the compensating centers, resulting in the appearance of a space charge field. These phenomena are described with the usual one-trap-one band model [9,10].

We solved the set of non-linear material rate differential equations [9,10], numerically for several values of fringe spacing, $\Lambda = 1, 2, 3, 4, 5, 7,$ and 10 microns. In this manner we obtained the variation of the overall space charge field as a function of light modulation for each value of the applied field (5 and 10 kV/cm). We followed the method described elsewhere [15,16]. For each of these values of fringe spacing we obtained the numerical solutions for several values of $m_0 = |m(z=0)|$, which is the value of the magnitude of light modulation at the surface of the sample between 0 and 1. Then we performed the Fourier decomposition for each of the calculated overall space charge field to obtain the amplitude, E_1, of its fundamental Fourier component and its phase, Φ, which is the phase shift of the space charge field with regard to the light interference pattern, for each of the cases considered. It is necessary to mention that this method does not rely on a Fourier expansion and so its validity is not limited by the use of a truncated harmonic basis. In this way we have obtained the grating strength and its phase, which are necessary to solve the beam coupling equations self-consistently, as functions of light modulation. The parameters used for the BSO are shown in Table I.

We considered a crystal cut to expose the $(\bar{1}10)$, the (110) and the (001) crystallographic faces. To deal with the two wave mixing (TWM) problem, we followed a tensor approach, taking into account optical activity, birefringence, absorption of light, for the two common optical configurations, the first with $K_G \parallel [001]$ and with light waves propagating in the $(\bar{1}10)$ plane. The second configuration is with $K_G \perp [001]$, where $K_G \parallel [\bar{1}10]$ and the light waves propagate in the (001) plane; the applied electric field is parallel to K_G For each configuration, the corresponding set of differential equations are obtained by the substitution of the light field, $\vec{A}(r)$ given by Eq. (1) and the electric displacement tensor, $\vec{D}(r)$, in the steady state wave equation,

$$\nabla^2 \vec{A}(r) + \frac{k_0^2}{\varepsilon_0}\vec{D}(r) = 0. \qquad (3)$$

$\vec{D}(r)$ in a sillenite medium can be expressed as

$$D_i = \varepsilon_0(\varepsilon_{ij} + G_{ij} + \Delta\varepsilon_{ij})E_j, \qquad (4)$$

where ε_{ij} is the symmetric optical permittivity tensor in the absence of optical activity and electro-optic coupling, G_{ij} is the tensor describing the optical activity, E_j is the j component of the electric field, and $\Delta\varepsilon_{ij}$ is the variation of the optical permittivity tensor induced by the linear Pockels electro-optical effect. The piezoelectric and photoelastic effects, for crystals of the sillenite family with the configurations we are considering can be neglected [12]. The permittivity and optical activity tensors are expressed in the light propagation coordinate system. Finally, the second derivative of the field is neglected In this manner the two sets of equations are obtained for the vectorial beam coupling: for $K_G \parallel [001]$ with the light waves propagating in the $(\bar{1}10)$ plane, and for $K_G \perp [001]$ and the light waves traveling in the (001)

TABLE I. Parameters for BSO and BTO [11, 16, 17-19] taken for our calculations.

		BTO	**BSO**
ε	Dielectric constant	47	56
n_0	Average refractive index	2.58	2.5
r	Electro optic coefficient (mV^{-1})	5.1×10^{-12}	4.7×10^{-12}
N_D	Donor density (m^{-3})	10^{25}	10^{25}
N_A	Acceptor density (m^{-3})	4×10^{22}	10^{22}
μ_τ	Mobility lifetime product ($cm^2 \, V^{-1}$)	6×10^{-7}	1×10^{-7}
γ	Recombination constant ($m^3 s^{-1}$)	1.6×10^{-17}	1.6×10^{-17}
s	Photo ionization cross section ($m^2 J^{-1}$)	1×10^{-5}	1×10^{-5}
α	Absorption coefficient (cm^{-1})		
	$\lambda = 532nm$	1.0	0.65
	$\lambda = 632nm$	0.3	0.30
ρ	Optical activity ($^{o} \, cm^{-1}$)		
	$\lambda = 532nm$,	100	386
	$\lambda = 632nm$	65	214

plane [11,12]. Absorption of light, optical activity and an external applied field parallel to the vector grating, are included in these two sets of equations.

The coupling factor, κ_1, is due to the space charge field obtained from the solution of the material rate equations, is complex, and is not constant throughout the sample thickness (z):

$$\kappa_1 = \frac{\pi \Delta n_1(x,z)}{\lambda \cos \theta} \qquad (5)$$

where $\Delta n_1(x,z)$ is the modulated change of the refractive index induced by the space charge field through the linear electro-optic effect:

$$\Delta n_1(x,z) = n_o^3 r \frac{|E_1(z)|}{2 |m(x,z)|} e^{i\Phi(z)} m(x,z) \qquad (6)$$

The phase shift of the space charge field with regard to the light interference pattern is Φ. Light beam propagation is along sample thickness and $m(x,z)$ is the complex light modulation, given by Eq. (2), $E_1(z)$ is the fundamental Fourier component of the space charge field; n is the average refraction index in the sample, λ is the wave length of the recording monochromatic beams, θ is the incidence Bragg's angle, and r is the electro-optic coefficient.

Notice that we are considering not only the magnitude of the variation of the refractive index along the sample thickness, but also the variation of its phase. It is important to take this into consideration when a static d.c. electric field is applied because the phase Φ is no longer $\pi/2$ as in the diffusion regime. The phase in this case is a function of both, the value of the applied field and the coordinate along the sample thickness.

During recording, the solutions to each set of beam coupling equations corresponding to $K_G \| [001]$ and $K_G \perp [001]$ must be self-consistent. This is because the changes in the intensities of waves and phases produce changes in the light modulation and on the refraction index. These changes, in turn, induce new changes in the intensity of the waves.

The set of beam coupling equations for $K_G \| [001]$ are [11,12]:

$$\frac{dA_{1\varsigma}(z)}{dz} = -\rho A_{1\xi}(z) - \frac{\alpha}{2} A_{1\varsigma}(z) \qquad (7a)$$

$$\frac{dA_{1\xi}(z)}{dz} = \rho A_{1\varsigma}(z)$$
$$+ i\kappa_0 A_{1\xi}(z) + i\kappa_1^*(z) A_{2\xi}(z) - \frac{\alpha}{2} A_{1\xi}(z) \qquad (7b)$$

$$\frac{dA_{2\varsigma}(z)}{dz} = -\rho A_{2\xi}(z) - \frac{\alpha}{2} A_{2\varsigma}(z) \qquad (7c)$$

$$\frac{dA_{2\xi}(z)}{dz} = \rho A_{2\varsigma}(z) + i\kappa_0 A_{2\xi}(z)$$
$$+ i\kappa_1(z) A_{1\xi}(z) - \frac{\alpha}{2} A_{2\xi}(z) \qquad (7d)$$

Here α is the absorption coefficient and ρ is the optical activity. The coupling factor κ_1 was defined in Ref. 5. The constant κ, is due to the variation of the magnitude of the change in the refractive index induced by the external applied field, E_0:

$$\kappa_0 = \frac{2\pi \Delta n_0}{\lambda \cos \theta} \qquad (8)$$

where

$$\Delta n_0 = \frac{n_0^3 r E_0}{2} \qquad (9)$$

Notice that κ_0 is not a function of z.

The set of beam coupling equations for $K_G \perp [001]$ are [11, 12]:

$$\frac{dA_{1\xi}(z)}{dz} = (\rho - i\kappa_0)A_{1\varsigma}(z)$$

$$- i\kappa_1^*(z)A_{2\varsigma}(z) - \frac{\alpha}{2}A_{1\xi}(z) \qquad (10a)$$

$$\frac{dA_{1\varsigma}(z)}{dz} = -(\rho + i\kappa_0)A_{1\xi}(z)$$

$$- i\kappa_1^*(z)A_{2\xi}(z) - \frac{\alpha}{2}A_{1\varsigma}(z) \qquad (10b)$$

$$\frac{dA_{2\varsigma}(z)}{dz} = -(\rho + i\kappa_0)A_{2\xi}(z)$$

$$- i\kappa_1(z)A_{1\xi}(z) - \frac{\alpha}{2}A_{2\varsigma}(z) \qquad (10c)$$

$$\frac{dA_{2\xi}(z)}{dz} = (\rho - i\kappa_0)A_{2\varsigma}(z)$$

$$- i\kappa_1(z)A_{1\varsigma}(z) - \frac{\alpha}{2}A_{2\xi}(z) \qquad (10d)$$

We solved each set of equations with no restrictions on the value of optical activity, nor on the coupling constant, and in a self-consistent way to take into account the variation with depth (this is z) of both the space charge field and light modulation. We divided the sample into thin layers of thickness Δz [16] in such a way that within each layer κ (z) is practically constant. In this way, within each layer we have analytical solutions [7] for the coupled equations of the two sets corresponding to $K_G \parallel$ [001] and $K_G \perp$ [001] When a small change (larger than 0.1%) in this variable occurred, we chose a smaller interval and calculated the new corresponding set of values of constants for the corresponding interval Δz. We started evaluating the initial set of constants for the first layer at the surface of the sample by using $\kappa(z = 0)$. Next, for the following layers, the values of the complex amplitudes of the beams at the end of each interval were used to evaluate m and therefore a new value of κ at z where the following layer starts.

We used gratings with different spatial periods, Λ, of 1, 2, 3, 4, 5, 7, and 10 microns several values of light modulation at the surface of the sample $m = 0.9, 0.6, 0.3$ and 0.1. We applied two fields: 5.0 and 10.0 kV/cm The values of absorption and optical activity used for BSO crystals are given in Table I. We also considered that the two beams were linearly polarized and had the same polarization angles at the surface of the sample when recording. The polarization angle is ϕ_p, defined as the inclination angle of the electric field of light waves with respect to the plane of incidence at the surface of the sample,

$$\varphi_{pi} = \tan^{-1}\left[\frac{A_{i\xi}(z=0)}{A_{i\xi}(z=0))}\right], \quad i = 1,2 \qquad (11)$$

From the complex amplitudes of light waves, obtained from the solutions of each set of equations, we calculated the intensities and phases of each wave as a function of z. For each one of the recording orientations we also obtained the diffraction efficiency η(z) defined as:

$$\eta(z) = \frac{I_d(z)}{I_i(0)} \qquad (12)$$

where I_d (z) =$|A_d$ (z) $|^2$ is the intensity of the diffracted light beam at the specific sample thickness z, and I_i (0) is the intensity of the incident light beam at the surface of the sample. The value of the diffracted intensity at the surface of the sample is I_d (z=0)=0.

3. Results and Discussion

Our calculations were performed using experimental data given in Table I for BSO and BTO. We considered absorption of light and optical activity.

In Fig. 1 we show the dependence of the diffraction efficiency on the sample thickness for a BTO grating. We used red light (632 nm) for reading; $K_G \perp$[001]; applied field E_0=5 Kv/cm. The polarization angle is $\Phi_p=\pi/2$ and m_0= 0.9. The absorption coefficient is 0.3 cm^{-1}. The grating was recorded with green light with an absorption coefficient of 1.0 cm^{-1} (see Table I). We can see clearly that, for all the values we used for the grating period, there is an optimal thickness. At this optimal thickness, the diffraction efficiency reaches a maximum value. The largest of these values is 28.6 % and occurs for the minimum value we considered for fringe spacing: 1 micron. The smallest value occurs for the largest value of the grating period: 10 microns.

In Fig. 2 we show the result for the dependence of the diffraction efficiency on the sample thickness for a BSO grating using red light (632 nm) for reading. For this case, $K_G \parallel$[001]; E_0= 10 Kv/cm; $\Phi_p = \pi/2$; m_0 =0.9;as in Fig. 1 the grating was recorded with green light (532 nm). The largest value of the diffraction efficiency is 54% and occurs for a grating period of 10 microns and a sample thickness of 1 cm. We can see that for all values of the grating period considered, the diffraction efficiency reaches a maximum value and
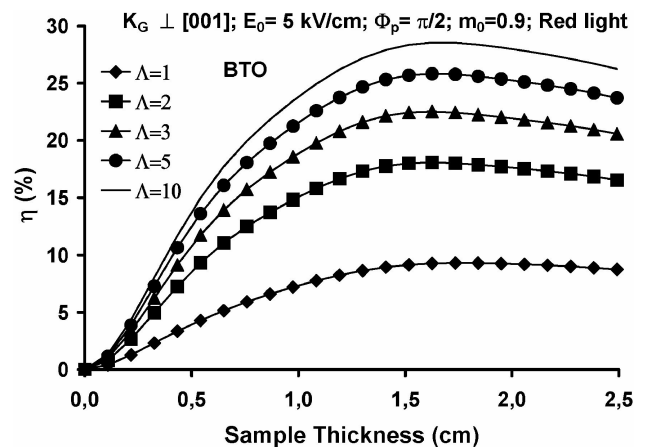
FIGURE 1. Result for the dependence of the diffraction efficiency on the sample thickness, for a BTO grating using red light (632 nm) for reading. For this case:$K_G \perp$[001]; E_0 =5 Kv/cm; $\Phi_p= \pi/2$; m_0 = 0.9.
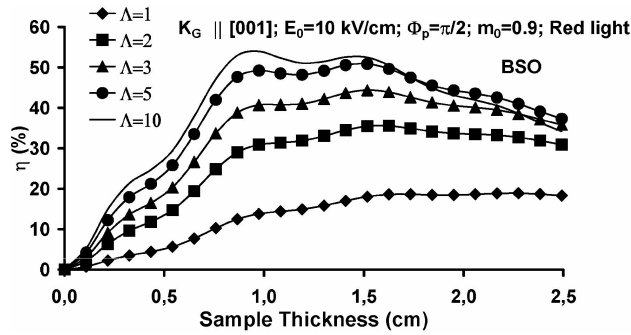
FIGURE 2. Result for the dependence of the diffraction efficiency on the sample thickness, for a BSO grating using red light (632 nm) for reading. For this case: $K_G \| [001]$; $E_0 = 10$ Kv/cm; $\Phi_p = \pi/2$; $m_0 = 0.9$.
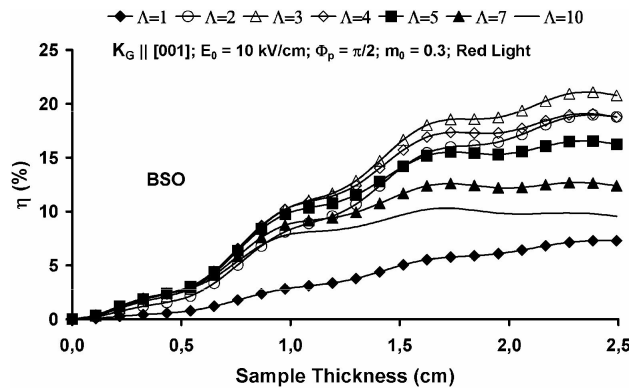
FIGURE 3. Result for the dependence of the diffraction efficiency on the sample thickness, for a BSO grating using red light (632 nm) for reading. For this case: $K_G \| [001]$; $E_0 = 10$ Kv/cm; $\Phi_p = \pi/2$; $m_0 = 0.3$.
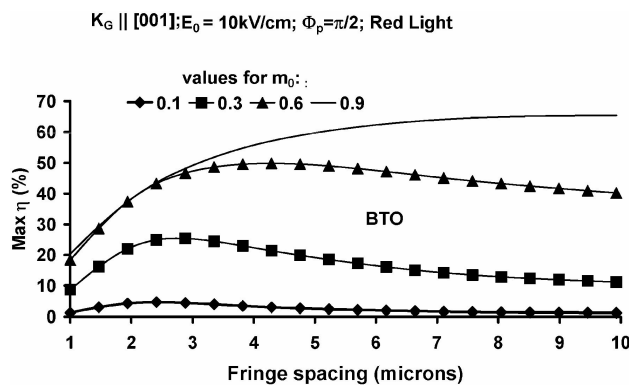
FIGURE 4. Result for the dependence of the maximum diffraction efficiency on the grating period for BTO, using red light (632 nm) for reading and different values for m_0(0.1, 0.3, 0.6 and 0.9). For this case: $K_G \| [001]$; $E_0 = 10$ Kv/cm; $\Phi_p = \pi/2$.
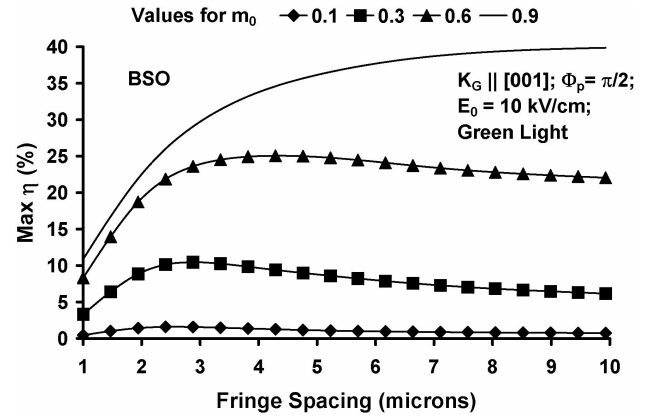
FIGURE 5. Result for the dependence of the maximum diffraction efficiency on the grating period for BSO using green light, 532 nm for reading and different values for m_0(0.1, 0.3, 0.6 and 0.9). For this case: $K_G \| [001]$; $E_0 = 10$ Kv/cm; $\Phi_p = \pi/2$.
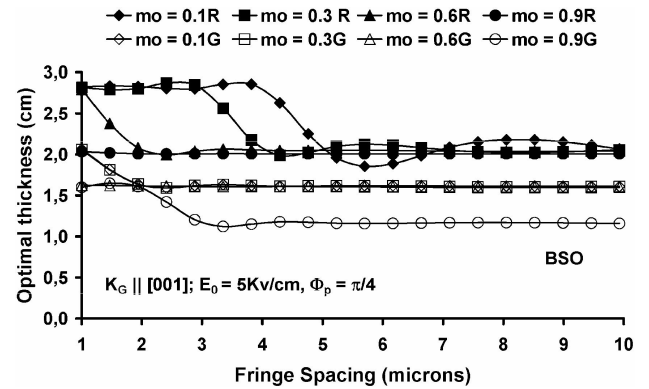
FIGURE 6. Dependence of the optimal thickness (to obtain the maximum diffraction efficiency), on the grating period for BSO using green light, 532 nm ($\blacklozenge$: $m_0 = 0.1$; $\blacktriangle$: $m_0 = 0.3$; $\bullet$: $m_0 = 0.6$; $\blacksquare$:$m_0 = 0.9$) and for red light, 632 nm ($\lozenge$:$m_0 = 0.1$; $\triangle$:$m_0 = 0.3$; $\circ$:$m_0 = 0.6$; $\square$:$m_0 = 0.9$), for reading. For this case: $K_G \| [001]$; $E_0 = 10$ Kv/cm; $\Phi_p = \pi/2$.
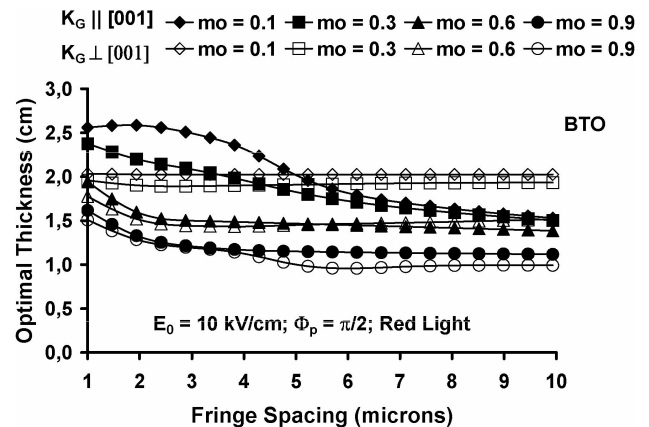
FIGURE 7. Dependence of the optimal thickness to obtain the maximum diffraction efficiency on the grating period for BTO using red light (632 nm) for reading. Two different sample orientations are considered. $K_G \| [001]$ ($\blacklozenge$:$m_0 = 0.1$; $\blacktriangle$:$m_0 = 0.3$; $\bullet$: $m_0 = 0.6$; $\blacksquare$:$m_0 = 0.9$) and, $K_G \perp [001]$ ($\lozenge$:$m_0 = 0.1$; $\triangle$:$m_0 = 0.3$; $\circ$:$m_0 = 0.6$; $\square$:$m_0 = 0.9$) For this case: $E_0 = 10$ Kv/cm; $\Phi_p = \pi/2$.

the smallest of these occurs for the smallest value of the grating period: 1 micron.

In Fig. 3 we show the result for the dependence of the diffraction efficiency on sample thickness for a BSO grating using red light (632 nm) for reading. For this case: $K_G\|[001]$; $E_0=10$ Kv/cm; $\Phi_p = \pi/2$; $m_0 = 0.3$. In this case, the largest value of the diffraction efficiency is 21% and occurs for a grating period of 3 microns and a sample thickness of 2.4 cm. We can see now that, for all the range of values of sample thickness considered, the grating period corresponding to 3 microns maintains the largest value for the diffraction efficiency. When the fringe spacing is 2 microns and the sample thickness increases, the diffraction efficiency increases more rapidly than in any other case. Notice now that for a fringe spacing of 10 microns, the diffraction efficiency reaches a maximum of 10.3% and then decreases. When the sample thickness is 2.5 cm, the value for the diffraction efficiency for a fringe spacing of 1 micron is close to the corresponding grating period value of 10 microns. This behavior is quite different from the one in Fig. 2, when m_0 was 0.9.

In Figs. 4 and 5 we show the dependence of the maximum diffraction efficiency on the grating period, for different situations for BTO and for BSO. In these figures the sample thickness is 2.5 cm.

In Fig. 4 we show the result for the dependence of the maximum diffraction efficiency on the grating period for BTO using red light (632 nm) for reading and different values for m_0(0.1, 0.3, 0.6 and 0.9). For this case: $K_G\|[001]$; $E_0=10$ Kv/cm and $\Phi_p = \pi/2$. We can see that the largest maximum value of the diffraction efficiency is 65.4 %, which occurs for an initial light modulation of 0.9. Notice that for every value of m_0 there is a grating period for which the maximum diffraction efficiency reaches its largest value; Thus the largest maximum value (4.7%) for $m_0 = 0.1$ occurs for a fringe spacing of around 2.5 microns; for $m_0 = 0.3$ the largest maximum (25.4%) happens when the grating period is 3 microns; for $m_0 = 0.6$ the largest value (49.9%) occurs when the fringe spacing is around 4 microns; when $m_0 = 0.9$ the diffraction efficiency increases when the grating period increases and reaches its saturation value (65.4%) when the grating period is around 7 microns.

Figure 5 shows the result for the dependence of the maximum diffraction efficiency on the grating period for BSO using green light (532 nm) for reading and different values for m_0(0.1, 0.3, 0.6 and 0.9). For this case: $K_G\|[001]$; $E_0=10$ Kv/cm ; $\Phi_p = \pi/2$. The overall behavior of the maximum diffraction efficiency is similar to the one in Fig. 4. The largest values of the maximum diffraction efficiency are smaller than the corresponding ones in Fig. 4. The largest value for the diffraction efficiency in this case is 40% for m_0=0.9. Again, the sample thickness in all cases is 2.5 cm. The value of the absorption coefficient for red light is smaller than the corresponding one for green light. This implied larger values for diffraction efficiency when reading with red light.

In Fig. 6 we show the influence of the color of the reading light on the value of the optimal thickness. We see here the dependence of the optimal sample thickness for obtaining the maximum diffraction efficiency on the grating period for BSO: for green light, 532 nm ($\blacklozenge$:m_0=0.1; $\blacktriangle$:m_0=0.3; $\bullet$:m_0=0.6; $\blacksquare$:m_0=0.9) and for red light, 632 nm ($\diamondsuit$:m_0=0.1; $\triangle$:m_0=0.3; $\circ$:m_0=0.6; $\square$:m_0= 0.9), for reading. For this case: $K_G\|[001]$; E_0=5 Kv/cm; Φ_p =$\pi/4$. It is interesting to notice the influence of the color of the reading light on the value of the optimal thickness. If we use green light the optimal thickness is the same (1.6 cm) for all values of m_0 except for m_0=0.9. In this latter case, the optimal thickness remains at 1.2 cm for a fringe spacing of 3 microns and larger. For smaller values of the grating period, the optimal thickness increase up to 2 cm. When we use red light, the optimal thickness increases for all cases and depends more strongly on m_0. For a grating period of 5 microns and larger the optimal thickness (2 cm) is about the same for all values of m_0. For values of the fringe spacing below 5 microns, we have a clear dependence on m_0. Thus, n this way for m_0=0.1 and m_0=0.3, the optimal thickness increases from 2 cm to 3 cm when the grating period goes from 5 to 1 micron. For m_0=0.6, the optimal thickness goes from 2 cm to 3 cm when the fringe spacing goes from 2 microns to 1 micron. Notice that there are some combinations of values of the parameters for which the optimal thickness is not sensitive to the value of the grating period.

Finally in Fig. 7 we show the dependence of the optimal thickness to obtain the maximum diffraction efficiency on the grating period for BTO using red light (632 nm) for reading. Two different sample orientation are considered: $K_G\|[001]$ ($\blacklozenge$: m_0=0.1; $\blacktriangle$: m_0=0.3; $\bullet$: m_0=0.6; $\blacksquare$: m_0=0.9) and, $K_G\perp[001]$ ($\diamondsuit$: m_0=0.1; $\triangle$: m_0=0.3; $\circ$: m_0=0.6;$\square$:m_0=0.9). For this case: E_0= 10 Kv/cm and Φ_p=$\pi/2$. We can see for both orientations that the higher the value of m_0, the more sensitive is the optimal thickness with a decreasing grating period. For both cases, when m_0 increases, the optimal thickness decreases for each value of fringe spacing.

4. Conclusions

We studied, under strong non-linear conditions the optimization of the diffraction efficiency in non-uniform gratings in BSO and BTO for thick samples with a small absorption coefficient. We used both red light and green light for reading. We considered variation of fringe period, optical activity, birefringence, absorption of light, and polarization angle. We included applied fields and considered two crystal orientations: in one the grating vector is parallel to the face [001], and in the other the grating vector is perpendicular to the same face. There is a complex relationship among all the parameters we have considered, and the prediction of the conditions for obtaining the optimum value of the diffraction efficiency is not simple. We have exhibited how this optimization can be obtained. There is always an optimal thickness to get the maximum diffraction efficiency for given

light modulation and grating period when recording. This optimal thickness is also dependent on the frequency and polarization of light, and on the sample orientation used for reading. There are some combinations of values of the parameters for which the optimal thickness is not sensitive to the value of the grating period. On the other hand, the grating period of 1 micron always corresponded to the smallest diffraction efficiency. The largest value for the diffraction efficiency was 65.4%. This was obtained for BTO with a fringe spacing of 10 microns, an initial light modulation $m_0 = 0.9$, and using red light for reading. The polarization angle was $\Phi_p = \pi/2 \ K_G||$ [001] and $E = 10$ kV/cm.

Acknowledgements

1. P. Gunter and J.P. Huignard, *Photo Refractive Materials and their Applications*,(Springer-Verlag, Berlin, 1988) vol. I; P. Gunter and J.P. Huignard, *Photo Refractive Materials and their Applications*, (Springer-Verlag, Berlin, 1989) vol. II.

2. P. Buchhave, S. Lyuksyutov, M. Vasnetsov, and C. Heyde, *J. Opt. Soc. Am. B* **13** (1996) 2595.

3. S.F. Lyuksyutov, P. Buchhave, and M.V. Vasnetsov, *Phys. Rev. Lett.* **79** (1997) 67.

4. S. Mallick, M.Miteva, and L. Nikolova, *J. Opt. Soc. Am. B* **14** (1997) 1179.

5. S.L. Hou, R.B. Laurer, and R.E. Aldrich, *J. Appl. Phys.* **44** (1973) 2652.

6. I. Foldvari, L.E. Halliburton, and G.J. Edwards, *Sol. Stat. Com.* **77** (1991) 181.

7. L.F. Magana, I. Casar, and J.G. Murillo, *Opt. Mater.* **30** (2008) 979.

8. I. Casar, J.G. Murillo, and L.F. Magana, *Physics Letters A* **352** (2006) 416.

9. N.V. Kukhtarev, G.E. Dovgalenko and V.N. Starkov, *Appl. Phys. A* **33** (1984) 227.

10. N.V. Kukhtarev, T.V.Kuktareva, J. Jones, E. Ward and H.J. Caulfield, *Opt.Comm.* **104** (1993) 23.

11. A. Marrakchi, R.V. Johnson, and J.A.R. Tanguay, *J. Opt. Soc. Am. B* **3** (1986) 321.

12. V.V. Shepelevich, N.N. Egorov, and V. Shepelevich *J. Opt. Soc. Am. B* **11** (1994) 1394.

13. VV. Shepelevich, S F. Nichiporko, A.E. Zagaorskiy, Yi Hu and A.A. Firsov, *Ferrolectrics* **266** (2002) 305.

14. B.I. Sturman, *et al.*, *Phys. Rev. E* **60** (1999) 3332.

15. J.G. Murillo, L.F. Magaña, M. Carrascosa and F. Agulló-López, *J. Opt. Soc. Am. B* **15** (1998) 2092.

16. J.G. Murillo, L.F. Magaña, M. Carrascosa and F. Agulló-López, *J. Appl. Phys.* **78** (1995) 5686.

17. C.L. Woods, C.L. Matson and M.M. Salour, *Appl. Phys. A* **40** (1986) 177.

18. J.P. Herriau, D. Rojas, and J.P. Huignard, *Ferroelectrics* **75** (1987) 271.

19. Y.F. Kargin, et al. *J. Cryst. Growth* **275** (2005) 779.